Nigerian Journal of Physics (NJP)
ISSN online: 3027-0936
ISSN print: 1595-0611
DOI: https://doi.org/10.62292/njp.v35i3.2026.650
Volume 35(3), September 2026

Hydrothermally Synthesized Doped Non-Aqueous Cds Thin Films for Degradation of Methylene Blue under Sunlight Radiation

[1]Owolabi Joseph Ayodele, [1,2]Aboritoli Sunday and [2,3]Femi David Matthew

[1]Department of Physics, Prince Audu Abubakar University Anyigba Kogi State Nigeria.
[2]Physics Department, Kogi State College of Education P.M.B. 1033, Ankpa, Kogi State Nigeria.
[3]Department of Physics & Astronomy, University of Nigeria, Nsukka, Enugu State, Nigeria.

*Corresponding Author's Email: Sunday4yemi@gmail.com Phone: +2348038544355

Keywords:
Cadmium sulfide,
Hydrothermal synthesis,
Non-aqueous medium,
Bismuth ferrite,
Tin oxide,
Photocatalysis,
Methylene blue,
Sunlight irradiation,
Thin films,
Dye degradation.

ABSTRACT

Cadmium sulfide (CdS) thin films have attracted significant attention for environmental remediation applications due to their suitable band gap, high photosensitivity, and excellent photocatalytic properties. In this study, non-aqueous CdS thin films were hydrothermally synthesized using cadmium nitrate tetrahydrate and thiourea as precursor materials in methanol medium. The films were prepared at varying precursor concentrations of 0.10 M, 0.20 M, and 0.30 M. To enhance the photocatalytic performance of CdS, 0/005g of bismuth ferrite ($BiFeO_3$) and 0.005g tin oxide (SnO_2) were incorporated as dopants in separate preparation. The synthesis was carried out in a Teflon-lined autoclave at 180 °C for 8 h, followed by washing, drying, and pulverization of the obtained products. The structural, morphological, optical, and photocatalytic properties of the synthesized samples were investigated using appropriate characterization techniques. The influence of precursor concentration and dopant incorporation on crystallite size, surface morphology, and optical band gap was evaluated. Photocatalytic activity was assessed through the degradation of methylene blue dye under natural sunlight irradiation. The results revealed that both $BiFeO_3$ and SnO_2 doping significantly improved the photocatalytic efficiency of non aqueoud CdS to 70.0 & 72.8% respectively by enhancing charge separation and reducing electron–hole recombination. The findings demonstrate that hydrothermally synthesized non-aqueous CdS thin films doped with $BiFeO_3$ and SnO_2 are promising photocatalysts for the degradation of organic pollutants in wastewater under sunlight irradiation, offering a cost-effective and environmentally friendly approach for water purification applications.

INTRODUCTION

Cadmium sulfide (CdS) belonging to II-VI group compound semiconductor has found potential interest due to its broad direct optical bandgap of approximately 2.42 eV and it high stability (Ankurkumar et al, 2018), it is a prominent semiconductor material widely studied for its applications in optoelectronic devices, including solar cells, photodetectors, and light-emitting diodes (Preeti, 2018). The synthesis of nanocrystalline CdS films through non-aqueous methods has garnered attention due to its unique properties compared to aqueous methods; (i) Higher purity, non-aqueous solvents minimize impurities and enhance the quality of CdS crystals. (ii) Controlled Morphology, non-aqueous allows for precise control over particle size and shape during synthesis, leading to tailored optical properties. (iii) Better Solubility, Non-aqueous solvents can dissolve a wider range of precursors, potentially improving the synthesis process. (iv) Enhance Stability, generally non-aqueous is more stable in the environments and also reduce degradation over time. (v) Improved Photocatalytic activity, non-aqueous exhibits better photocatalytic properties due to reduced electron-hole pair recombination (Suresh, 2018). Doping CdS with foreign elements is a common strategy to tune its electrical and optical properties. Among various dopants, (Sn), a group iv element has shown promising results in modifying charge carrier density and band structure. Nanocrystalline forms of CdS shown quantum confinement effects, allowing tunable optical properties, which are highly beneficial in nanoscale

device engineering (Preeti, 2018, Yakubu, etal., 2026). Non – aqueous synthesis routes, using organic solvents and precursors, offer an alternative approach with several advent stages like controlled nucleation, reduced agglomeration, and inhibition of oxide formation. In cadmium sulfide based solar cells like zinc sulfide (ZnS) and cadmium in zinc sulfide (CdZnS) could lead to decrease in window absorption loses and equally improve the short circuit current of the cell (Suresh, *etal*., 2016), cadmium sulfide thin films have been deposited by several methods like vacuum evaporation, electrodeposition, chemical bath deposition, sputtering, spray hyrolysis and laser abalative (Dariani & Emani, 2015).

Non –aqueous synthesis routes ring organic solvents and precursors, offer an alternative approach with several advantage, controlled nucleation, reduced agglomeration and inhabitation of oxide formation (Farimia et al, 2021). Traditional aqueous methods of CdS synthesis often suffer from limitations such as poor control over crystallinity, contamination, and film uniformity. Non – aqueous deposition teaching us, especially in organic solvents, provide better control over nucleation and growth kinetics, enabling it fabrication of high- purity nanocrystalline films with tailor properties Wesam, etal., (2024).

Hydrothermal processing has several advantages over both traditional and cutting-edge synthesis methods. (1) Compared to other cutting-edge methods, the cost of precursors, energy, and equipment is significantly lower. (2) Simple and safe for the environment. (3) The particle size and form may be effectively controlled. (4) Using this method, crystalline phases that are unstable at their melting temperatures can also be generated. In addition to being utilized for the synthesis of materials with high vapour pressures at melting temperatures, this process can also be used to produce huge, high-purity crystals with precisely regulated compositions. (7) Reducing damages. One drawback is the inability to watch the crystal as it grows. Influenced by temperatures and pressures below the solvent's critical point (Shukla & Rani, 2023).

Approximately half of all dyes made and used worldwide are aromatic azo dyes. Fifteen percent of the dyes used in various industries are released into aquatic environments. Azo dyes have the potential to cause cancer, allergic reactions in the skin and eyes, and breathing issues. (Delima, et al., 2007). These pollutions are being removed by using various methods such as biodegradation, chlorination, flocculation, ozonation, and photocatalytic degradation. Azo Dye are not biodegradable while other methodologies produce secondary pollutants except photocatalytic degradation which does not produce secondary pollutants (Ata, et al., 2023).

The utilization of the photocatalytic degradation approach is favoured due to its eco-friendly nature and reduced production of hazardous compounds. This method is based on how radiation interacts with a nanocatalyst surface and oxidative reagents; it is created when pollutants degrade (Somwanshi, et al., 2023).

In this work we doped non aqueous CdS at different concentration deposited by hydrothermal with bismuth ferrite and tin oxide to improve on phocatalytic activities, energy bandgap, and surface area, oxygen adsorption on the surface and electron and whole recombination.

Preparation of Non-Aqueous CdS Thin Film by Hydrothermal Technique Doped with Bismuth Ferrite and Tin Oxide

Different concentrations (0.10 M, 0.20 M, and 0.30 M) of cadmium nitrate tetrahydrate were prepared in separate conical flasks. The solutions were prepared using appropriate volumes of methanol. Each solution was stirred at 250 rpm for 30 minutes, after which 0.5 g of thiourea was added, and stirring was continued for another 30 minutes. Subsequently, triethanolamine was added, and the mixture was stirred for an additional 30 minutes. The resulting solution was then transferred into a 100 mL Teflon-lined autoclave and heated in a muffle furnace at 180 °C for 8 hours. The obtained product was washed with distilled water, dried in an oven at 70 °C for 6 hours, and then crushed into a fine powder.

The same procedure was repeated with the addition of 0.005 g of bismuth ferrite as a dopant to the 0.10 M, 0.20 M, and 0.30 M cadmium nitrate tetrahydrate precursor solutions, respectively. Furthermore, the procedure was repeated with the addition of 0.005 g of tin oxide as a dopant to the 0.10 M, 0.20 M, and 0.30 M cadmium nitrate tetrahydrate precursor solutions, respectively.

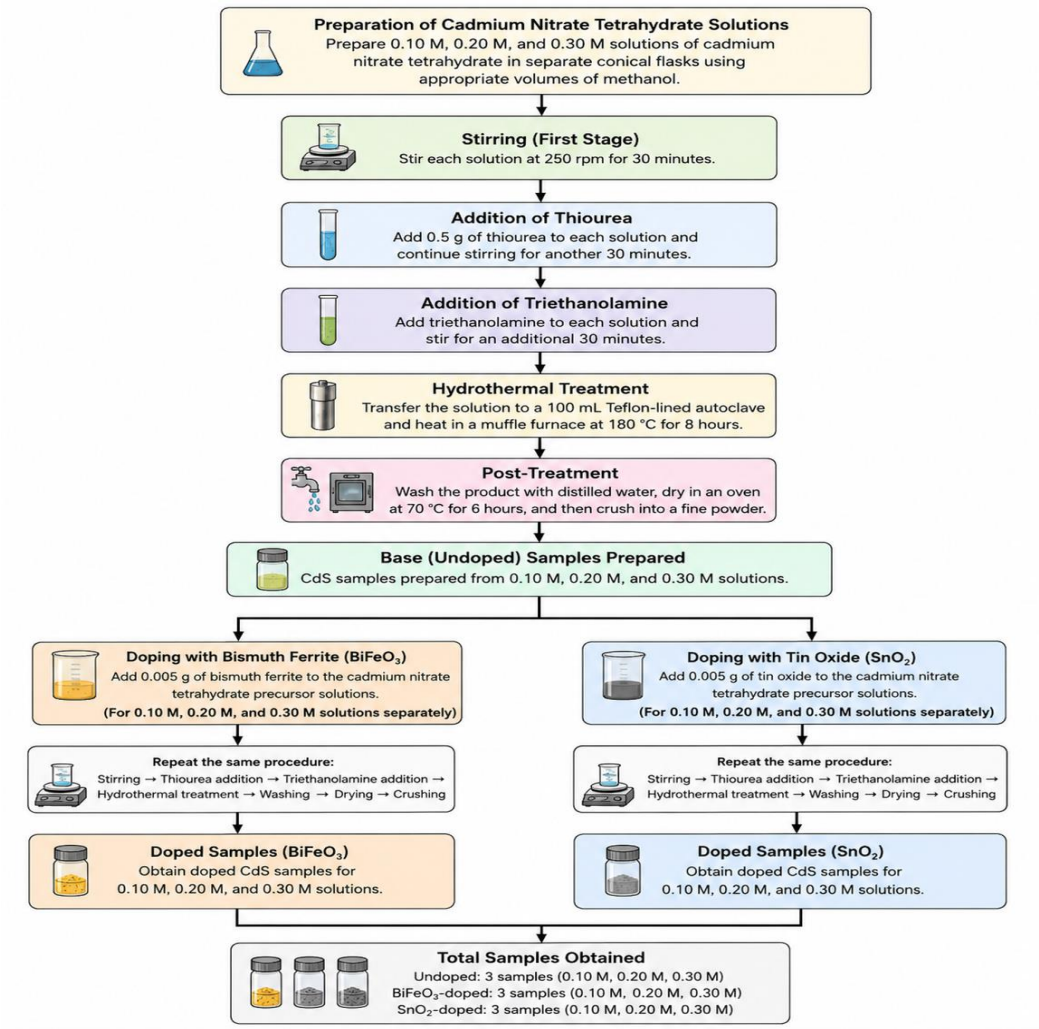

Plate 1: Flow Chart for the Preparation of Undoped and Doped Non-Aqueous CdS

X-ray Spectroscopy Results for Non-Aqueous CdS Deposited by Hydrothermal Technique Doped with Bismuth Ferrite and Tin Oxide at Different Concentration

The X-ray diffraction (XRD) patterns of non-aqueous CdS deposited at 0.1 M, 0.2 M, and 0.3 M concentrations, respectively, using the hydrothermal technique with JCPDS reference codes 96-900-4179, 92-900-4479, and 96-900-4279 are illustrated in Figure 1. It can be observed that the number of diffraction peaks decreases as the concentration of non-aqueous CdS increases for all the samples.

When the samples were doped with bismuth ferrite, as illustrated in Figure 2. The effect of the doping became evident through the increase in peak intensities in all the samples. However, the preferred peak position (2θ) of the $BiFeO_3$-doped non aqueous CdS decreased with increasing concentration, that is, from 30° at 0.1 M to 27° at 0.2 M and 13° at 0.3 M.

When the samples was doped with tin oxide as illustrated in Figure 3, the prefer peak shifted to lower 2θ for all the samples at different concentration. Similar result was obtained in Figure 2 when non aqueous CdS was doped with bismuth ferrite. The samples doped with tin oxide contained a lot of noise, the present of noise associated with the samples doped with tin oxide as compared to the sample doped with bismuth ferrite may be ascribed to effects of different in dopant.

The crystallite size (D) of non-aqueous CdS deposited by hydrothermal method, doped with bismuth ferrite and tin oxide at difference concentration were calculated with the Debye-Scherrer formula

$$D = \frac{k\lambda}{\beta cos\Theta} \quad (1)$$

(Tasdemirci, 2019) Where K is a dimensionless shape factor of 0.94, λ is the wavelength of X-ray of 0.154nm, β is the full width at half maximum (FWHM) of a diffraction peak in radian and θ is the Bragg angle. The crystallite sizes of non-aqueous CdS deposited by

hydrothermal, doped with bismuth ferrite and tin oxide at difference concentration are showed in table 1.

The dislocation density was calculated from

$$\alpha = \frac{1}{D^2} \quad (2)$$

(Ikram et al., 2020), where D is the crystallite size and α is the dislocation density.

The crystallite size increases as the concentration of non-aqueous CdS increases for both synthesis doped and undoped samples. This may be because a higher concentration provides more ions for crystal growth. Increased concentration also enhances collisions among particles, which promotes aggregation and grain growth, thereby increasing the crystallite size and consequently leading to larger particle sizes.The Miller indices obtained in this work are similar to those reported by Dariari and Emane (2015).

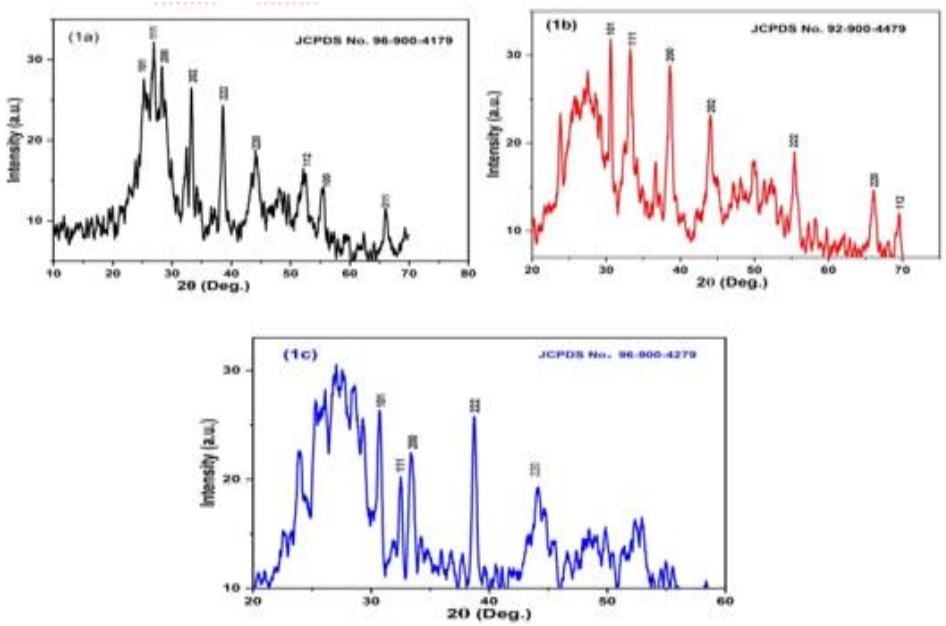

Figure 1: 1a, 1b, & 1c represents the X-ray spectroscopy results for non-aqueous CdS at 0.1m, 0.2m, & 0.3m respectively

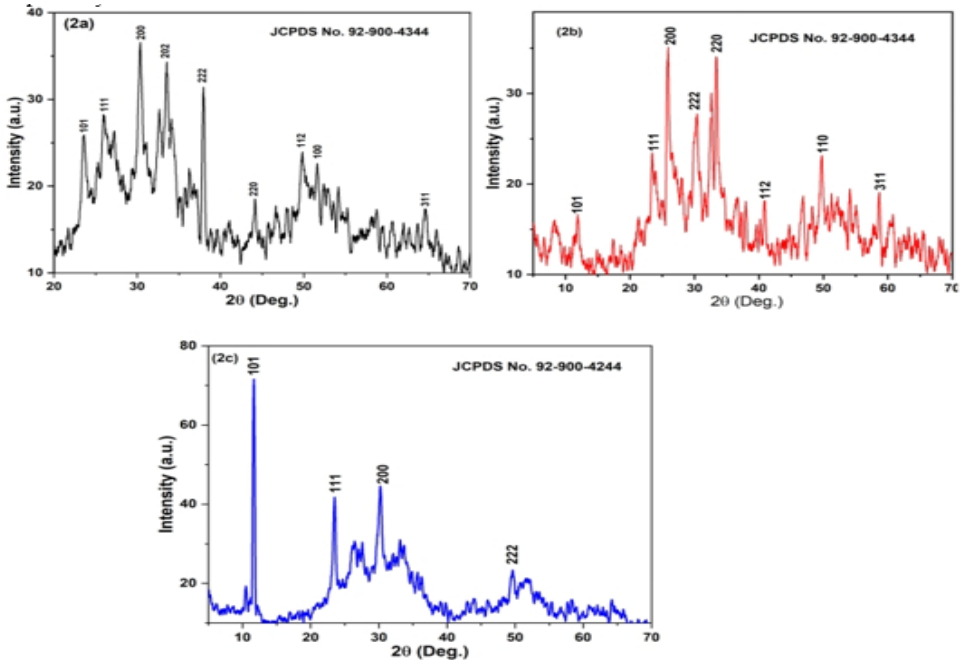

Figure 2: 2a, 2b, & 2c represents the X-ray Spectroscopy Results for Non-Aqueous CdS Doped with Ferrite at 0.1m, 0.2m, & 0.3m respectively

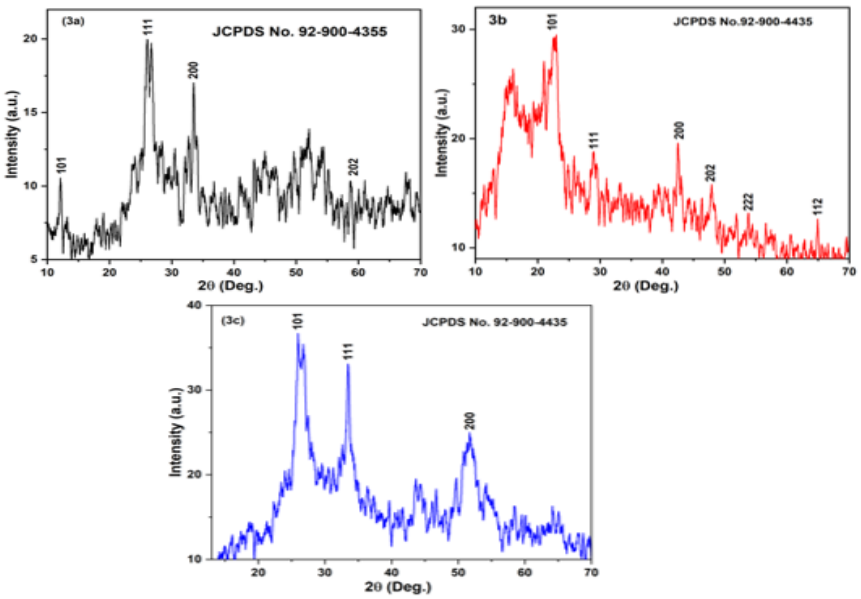

Figure 3: 3a, 3b, & 3c Represents the X-ray Spectroscopy Results for Non-Aqueous CdS Doped with Ferrite at 0.1m, 0.2m, & 0.3m Respectively

Table 1: Crystallite Sizes and Dislocation Density for Undoped, Doped Aqueous Cds with Bismuth Ferrite & Tin Oxide at Difference Concentration Respectively

Concentration	Undoped non-aqueous CdS		Doped non-aqueous CdS with bismuth ferrite		Doped non-aqueous CdS with tin oxide	
	Crystallite size (nm)	Dislocation density $(nm)^{-}$	Crystallite size (nm)	Dislocation density $(nm)^{-}$	Crystallite size (nm	Dislocation density $(nm)^{-}$
0.1M	2.45	0.1666	2.95	0.1149	3.01	0.1104
0.2M	2.62	0.1457	3.42	0.0855	3.54	0.0798
0.3M	2.74	0.1332	3.87	0.0668	3.98	0.0631

Scanning Electron Microscopy Results for Non-Aqueous CdS Deposited by Hydrothermal Technique Doped with Bismuth Ferrite and Tin Oxide at Different Concentration

SEM micrographs in Figure 4 Revealed irregular granular morphology with varying degrees of agglomeration among the samples which may be attributed to different in concentration of the samples. Sample 1A exhibited a relatively dense and homogeneous microstructure with finer particles and reduced porosity, indicating improved particle dispersion and packing. In contrast, sample 1B showed larger agglomerates and a rough heterogeneous surface, suggesting incomplete dispersion and increased porosity. Sample 1C demonstrated intermediate characteristics with moderate particle uniformity and agglomeration. The observed microstructural differences are expected to influence the physical and mechanical properties of the material.

SEM analysis in Figure 5 revealed that sample 2A possesses finer and more compactly distributed grains, while sample. In contrast sample 2B showed larger cracked agglomeration with rough heterogeneous surface 2C exhibits largest agglomerated clusters with roughest surface morphology. The increase in particle aggregation and grain growth in sample 2C suggests an increase in crystallite size and reduced structural uniformity. The different in morphology observed in Figure 4 and Figure 5 may be attributed to the varies concentration and present of dopant.

SEM analysis in Figure 6, sample 3A shows fine, uniformly distributed particles with a relatively smooth and compact surface, indicating smaller grain size and lower porosity. In contrast, sample 3B exhibits larger and more irregular crystalline grains with visible voids and pores, suggesting higher porosity and a rougher surface morphology. Sample 3C displays highly agglomerated and compact clustered particles with a denser and rougher texture than 3A, indicating increased particle interaction and agglomeration. Overall, the morphology changes from finer and more homogeneous particles in 3A to larger porous grains in 3B and finally to densely agglomerated structures in 3C. The different in morphology may be attributed to different in concentration and nature of dopant.

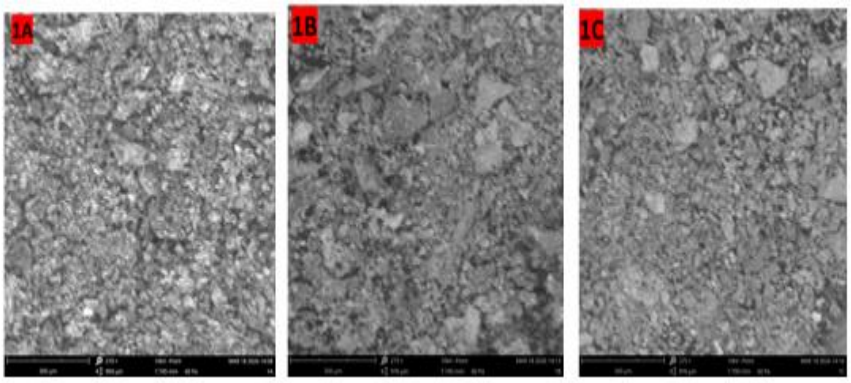

Figure 4: 1A, 1B & 1C represent Scanning Electron Microscopy Images of non-aqueous CdS at concentration of 0.1m, 0.2m, & 0.3m respectively

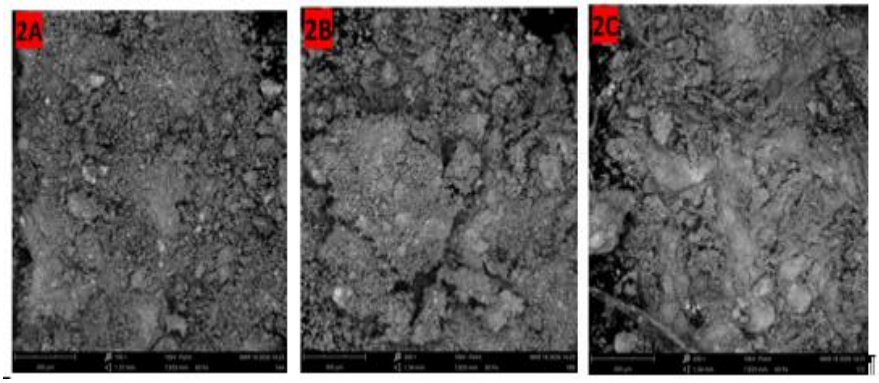

Figure 5: 2A, 2B & 2C represent Scanning Electron Microscopy Images of non-aqueous CdS at concentration of 0.1m, 0.2m, & 0.3m respectively doped with bismuth ferrite

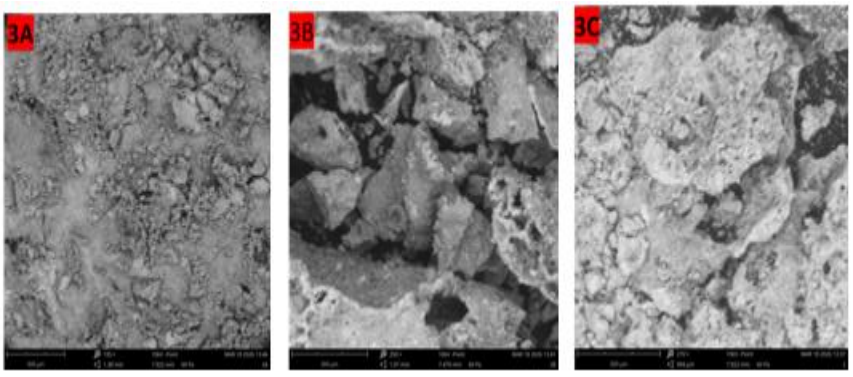

Figure 6: 3A, 3B & 3C represent Scanning Electron Microscopy Images of non-aqueous CdS at concentration of 0.1m, 0.2m, & 0.3m respectively doped with tin oxide

UV -Visible Spectroscopy Results for Non-Aqueous CdS at Varying Concentration Doped with Bismuth Ferrite and Tin Oxide at Different Concentrations

Figure 7 describes the absorbance and direct energy band gap of non-aqueous CdS deposited using the hydrothermal technique at different concentrations. The results obtained were (275 nm, 3.9, 4.0 eV), (255 nm, 3.9, 3.9 eV), and (255 nm, 3.9, 3.7 eV) for wavelength, absorbance, and energy band gap at concentrations of 0.1m, 0.2m, & 0.3m, respectively.

The direct band gap nature, as shown in the inset, was calculated using the Tauc plot method (Nkele et al., 2020; Ikhioya et al., 2023). The variation in energy band gap values is attributed to changes in concentration. As the

concentration of non-aqueous CdS increases, the energy band gap decreases. The pattern of variation in energy band gap obtained in this work is similar to that reported by Matthew et al. (2024). All the samples exhibited the same absorbance value of 3.9 within the wavelength range of 225–275 nm.

Figure 8 describes the absorbance and direct energy band gap of non-aqueous CdS doped with bismuth ferrite and deposited using the hydrothermal technique. The results obtained were (270 nm, 3.7, 3.8 eV), (280 nm, 3.9, 3.7 eV), and (285 nm, 3.9, 2.8 eV) for the different concentrations studied.

The results revealed that the energy band gap of the doped CdS decreases as the concentration increases. This reduction in band gap may be attributed to the incorporation of bismuth ferrite into the CdS matrix, which enhances the electronic interaction and modifies the optical properties of the material. The results obtained in this work are similar to those reported by Dariari and Emane (2015).

Figure 9 describes the absorbance and direct energy band gap of non-aqueous CdS doped with tin oxide and deposited using the hydrothermal technique at different concentrations. The results obtained were (260 nm, 3.8, 3.5 eV), (255 nm, 3.8, 3.2 eV), and (255 nm, 3.8, 3.0 eV) for wavelength, absorbance, and energy band gap at concentrations of 0.1m, 0.2m, & 0.3m respectively.

The energy band gap of the doped non aqueous CdS decreases with increasing concentration. The energy band gap values of the samples doped with bismuth ferrite were slightly lower than those samples doped with tin oxide as shown in Table 2.

The as-deposited non aqueous CdS exhibited a maximum absorbance value of 3.8 for all the doped samples synthesized at varying concentrations within the wavelength range of 255–260 nm. This value is slightly lower than that obtained for undoped samples the variations observed in wavelength at maximum absorbance values, and energy band gap may be attributed to differences in sample concentration and variation in dopant employed.

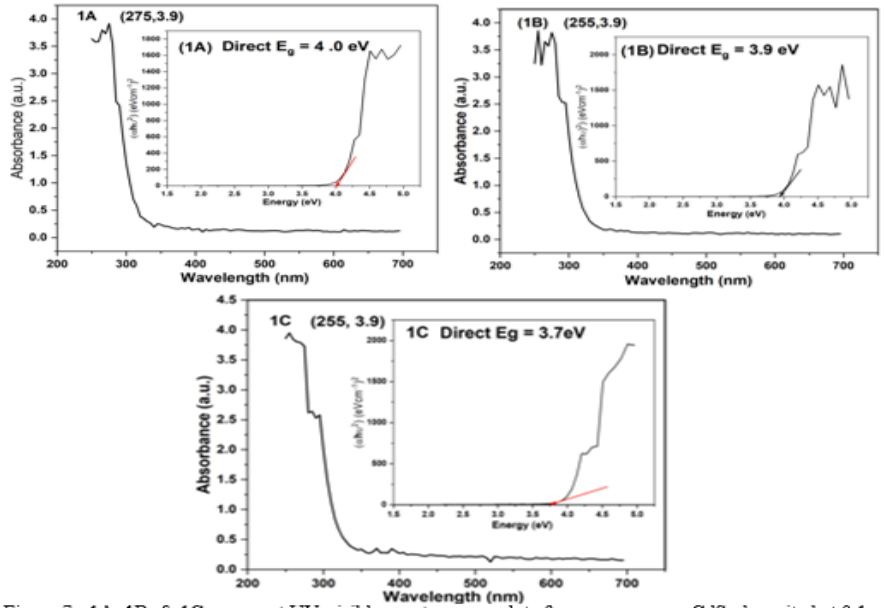

Figure 7: 1A, 1B, & 1C represent UV-visible spectroscopy plots for non aqueous CdS deposited at 0.1m, 0.2m, & 0.3m respectively

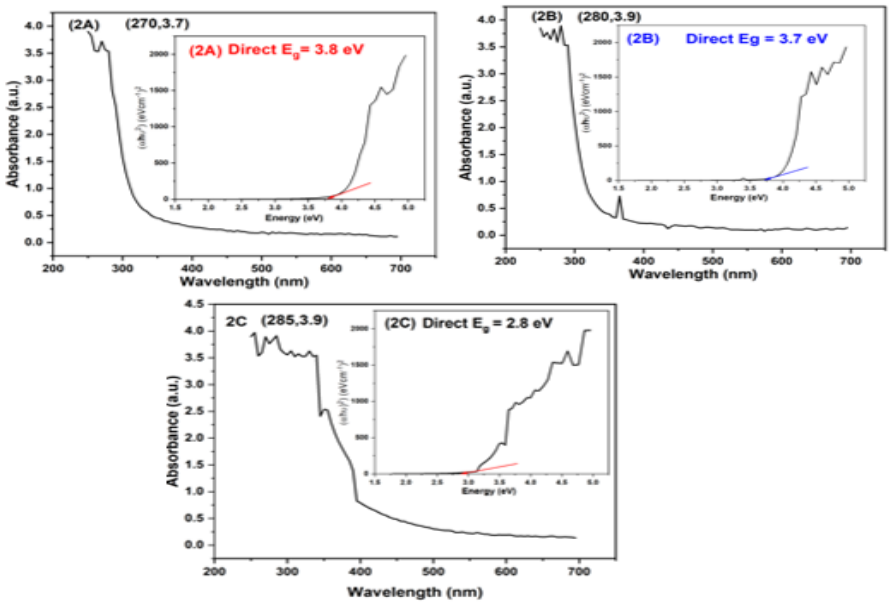

Figure 8: 2A, 2B, & 2C represent UV-visible spectroscopy plots for non aqueous CdS doped with bismuth ferrite at varying concentration of 0.1m, 0.2m, & 0.3m respectively

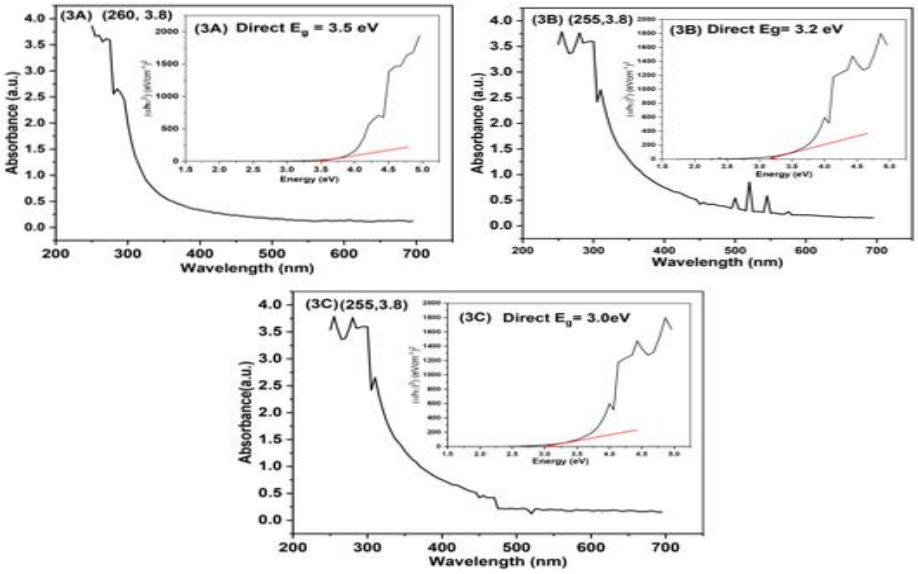

Figure 9: 3A, 3B, & 3C represent UV-visible spectroscopy plots for non aqueous CdS doped with tin oxide at varying concentration of 0.1m, 0.2m, & 0.3m respectively

Table 2: Concentration, Absorbance, Wavelength and Energy Band Gap of Undoped and Doped CdS with Bismuth Ferrite and Tin Oxide

Concentration	Undoped CdS			CdS doped with $BiFeO_3$			CdS doped withSnO_2		
	Abs,	λ (nm)	E_g (eV)	Abs,	λ (nm)	E_g (eV)	Abs,	λ (nm)	E_g (eV)
0.1 M	3.9	275	4.0	3.7	270	3.8	3.8	260	3.5
0.2 M	3.9	255	3.9	3.9	280	3.7	3.8	255	3.2
0.3 M	3.9	255	3.7	3.9	285	2.8	3.8	255	3.0

Photocatalytic Degradation Properties of Undoped and Doped Non-Aqueous CdS with Bismutg Ferrite and Tin Oxide at 2M Concentration under Sunlight Radiation

The photoactivity measurements of undoped and doped non-aqueous CdS at 2 M concentration, deposited using hydrothermal under sunlight radiation, are illustrated in Figures 10 as well as in Table 2. The degradation efficiencies of 10 mg nanoparticles for the degradation of 10 ppm methylene blue at a degradation interval of 30 minutes were 41.14%, 72.78%, and 70.01% for undoped and doped non-aqueous CdS with bismuth ferrite and tin oxide deposited using the hydrothermal methods, respectively, under sunlight radiation.

From the results, it can be deduced that the degradation efficiency increased when the non-aqueous CdS was doped with bismuth ferrite and tin oxide. However, the degradation efficiency was slightly higher for non-aqueous CdS doped with bismuth oxide compared to non-aqueous doped with tin oxide. The highest percentage of degradation for the doped samples occurred within the first 30 minutes of exposure time. The study revealed that the nature of the dopants and the synthesis methods significantly affect the degradation efficiency of non-aqueous CdS.

The reaction rate equation [$\ell n(C_o \backslash C_t) = Kt$] gives the relationship between ln(Co\Ct) and the exposing time t from which the pseudo-first order rate constant K was determined (Ali et al.,2021).

From the equation; C_o is the concentration at an exposing time of zero while C_t is the concentration at an exposing time t. The graph of this relation is illustrated in Figure 4.15. The slope of the graph represents the pseudo-first order rate constant (K) with obtained values as 0, 0057 per min, 0.0 136 per min, & 0.0132 per min for undoped and doped non-aqueous CdS with bismuth ferrite and tin oxide at 2M concentration. The pseudo- first order rate constant of the doped non aqueous CdS is within the range of 0.0132 to 0.0136 per min.The results obtained confirmed the ability of the doped non aqueous CdS to generate holes and electrons that we speed up degradation process.

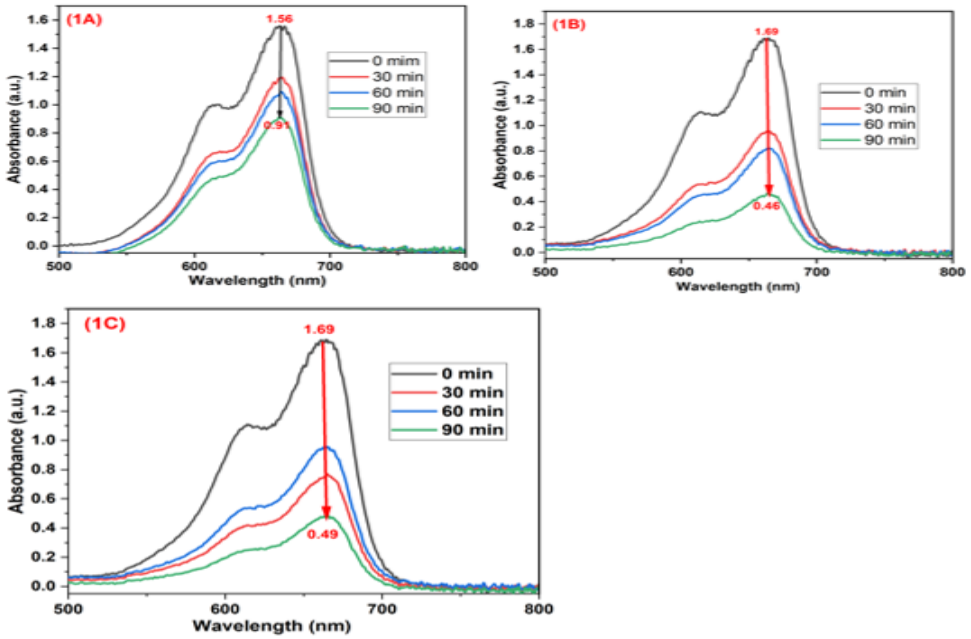

Figure 10: 1A, 1B & 1C represent Photocatalytic degradation Properties of undoped and doped non aqueous CdS with bismuth ferrite and tin oxide at 0.2M concentration under sunlight radiation

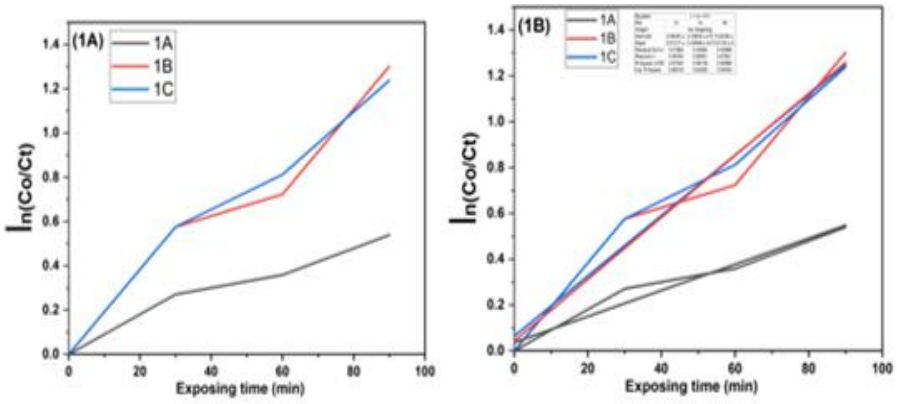

Figure 11: 1A & 1B, Plots of unfitted and fitted first order rate constant for non-aqueous CdS and doped non aqueous CdS with bismuth ferrite and tin oxide at concentration of 0.2 M under sun light radiation

Table 3: Exposing Time and Degradation Efficiency of Undoped and Doped Non Aqueous Cds with Bismuth Ferrite and Tin Oxide at 0.2M Concentration under Sunlight Radiation

Exposing time (Min)	Samples Degradation efficiency in %		
	1A	1B	1C
0	0	0	0
30	23.7	43.8	43.8
60	30.8	51.5	54.4
90	41.1	72.8	70.0

CONCLUSION

In this study, non-aqueous cadmium sulfide (CdS) thin films were successfully synthesized through the hydrothermal method using precursor concentrations of 0.10 M, 0.20 M, and 0.30 M. The synthesized CdS samples were further modified by doping with bismuth ferrite ($BiFeO_3$) and tin oxide (SnO_2) to improve their photocatalytic performance. The effects of precursor concentration and dopant incorporation on the structural, morphological, optical, and photocatalytic properties of the samples were investigated.The characterization results demonstrated that variations in precursor concentration significantly influenced the crystallite size, surface morphology, and optical properties of the CdS thin films. Doping with $BiFeO_3$ and SnO_2 enhanced the crystallinity and modified the electronic structure of CdS, leading to improved light absorption and more efficient charge carrier separation. The reduction in electron–hole recombination contributed to enhanced photocatalytic activity under sunlight irradiation. Photocatalytic degradation studies using methylene blue dye revealed that both $BiFeO_3$- and SnO_2-doped CdS samples exhibited superior degradation efficiencies compared to the undoped CdS samples. The improved photocatalytic performance was attributed to the synergistic effects of the dopants, which increased the number of active sites and facilitated charge transfer processes. Among the investigated concentrations, the optimum concentration exhibited the highest photocatalytic degradation efficiency, indicating that precursor concentration plays a crucial role in determining the photocatalytic behavior of the synthesized materials. Overall, the study confirms that hydrothermally synthesized non-aqueous CdS thin films doped with $BiFeO_3$ and SnO_2 are effective photocatalysts for the degradation of methylene blue under natural sunlight irradiation. The findings demonstrate the potential of these materials for environmental remediation and wastewater treatment applications. Furthermore, the use of sunlight as the irradiation source provides an economical and environmentally sustainable approach for the removal of organic pollutants from contaminated water.

REFERENCES

Ali, S. M., Dakhil, O. A, & Hussein, E.H. (2021). Modified hydrothermal preparation of ZnO/NiO nanojunction for enhancement of photocatalytic activity. Journal of Acta physical polonica, vol. 140, issue 1.

Ankurkumar, J. K., Sunil H. C., Tasmira, J. M, Jiten P. T., Sanjaysinh, M. C. & Deshpande, M.P. (2018). Cadmium sulphide (CdS) thin films deposited by chemical bath deposition (CBD) and dip coating techniques - a comparative study. Journal of material science express, vol. 10 pp1-22, https://doi.org/10.1088/2053-1591/aab28d

.Ata, S., Shaheen,I., Aslam, H., Mohsin, I.U., Alwadai, N., Huwayz , M.A., Iqbal, M., & Younas, U. (2023). Barium and strontium doped La -based perovskite synthesis via sol-gel route and photocatalytic activity evaluation for methylene blue. Journal of homepage Physics, vol. 45, p. 106235.

Dariari & Emane (2015). Structural and optical studies of CdS and CdS : Ag nano needles prepared by a SILAR method, ceramic international journal, vol 3, pp.111-119. http://dx.doi.org/10.1016/j.ceramint.2015.03.111

Delima, R. O., Bazo, A.P., Salvadori, D.M.F., Pech, C. M. Oliveira, D. P. & Umbuzeiro, G.A. (, I.O. (2025). Influence of Silicon Nanoparticle on the Electrical Properties of Heterostructured 2007). Muta genic and carcinogenic potential of textile azo dye processing plant effluent that impacts a drinking water source. Journal of Toxicology and Environmental Mutagenesis. Vol. 626, pp.53-60.

Faremia, A. A., Oluyamob, S. S., Adedayo, K. D., Odusoteb, Y. A. & Olusola CdTe/CdS thin films based Photovoltaic Device. Journal of the Nigerian Society of Physical Sciences, vol.3, pp256-261

Ikhioya, J. L. & Nkele, A. C. (2023). A Novel synthesis of hydrothermally prepared europium sulfide and cerium sulfide nanomaterials doped with yttrium.Arab journal of science engineering, vol. 23, pp. 08292-08299.

Ikram, R., Jan, B. M. & Ahmad, W. (2020) An overview of industrially scalable production of graphene oxide and analytical approaches for synthesis and characterization. Journal of materials research and Technology vol. 9, pp. 11587-11610, https://doi.org/10.1016/j.jmrt.2020.08.050.

Matthew, D.F., Jain, H.G., Nkele, A.C., Shinde, S.D., Azeez, A.A., Manoj A. More, Huda I. Ahmed., Ahr.Y. B., Sonawane, L.D., Adil Alshoaibi., Ezekoye, B.A., Ekwealor, A.B.C., Fabian I. Ezema, Dnyaneshwari Y. Patil. And Ganesh E. Patil1. (2024). Investigating the properties of GO/(ZnxNi1−x) O composites prepared by Sol–gel route for photocatalytic and gas sensing applications, Journal of material science and material in electronic, vol. 4 pp 1-14. https://doi.org/10.1007/s10854-024-13262-4 .

Nkele, A.C., Chine,U., Ezealigo, B., Nwanya,A., Agbogu, A. C., Ekwealor,A.B.C., Osuji, R. U., Ejikeme, P.M., Maaza, M. & Ezema,F.I. (2020). Enhanced electrochemical property of SILAR deposited Mn3O4 thin films decorated on graphene. Journal of materials research and technology vol.9, pp. 9049-9058.

Preeti, S. (2018). Synthesis and Characterization oc CdS Nanoparticle. International Journal of Engineering research & technology, vol, 2 issue 6, pp 24-32.

Shukla, D., & Rani, S. (2023). Effect of autoclave and non-autoclave hydrothermal synthesis methods on the structural properties and optical properties of LiBaF3 phosphor: A comparative study. Journal of Materials today, vol. 4, pp. 147-152, https://doi.org/10.1016/j.matpr.2023.04.147.

Somwanshi, S.B., Kharat, P.B. & Thorat, N. D. (2021). Magnetically Retrievable Fe-doped TiO2 Nanoparticles for photo-induced toxic dye removal applications. Macromolecular symposia, Willey online Library pp. 421-429.

Suresh, P. (2018). Preparation and Characterization of bismuth ferrite nanoparticles. Materias Today: proceedings, vol,5, pp 876- 882.

Suresh, K., S. Sharma, K Shashikant, R., S. Kumar, R., Srikant, S. & Roy, D. (2016). Synthesis and Characterization of Nonaqueous Deposited Nanocrystalline Cds Film. International Journal of Advanced Engineering Research and Science, vol.3 pp 61 -65.

Tasdemirci, T.C. (2019). Influence of annealing on properties of SILAR deposited nickel oxide films. Journal of Vacuum, vol. 169, pp. 189-194 https://doi.org/10.1016/j.

Wesam, A. E., Naoufel, B. H., Mohamed,.G., El, D. & Ahmed, S. (2024). A green synthesis of cellulose nanocrystals biosorbent for remediation of wastewater containing industrial dye. Colloids and surface A: Physicochemical and Engineering Aspects, vol. 681, p132729 https://doi.org/10.1016/j.colsurfa.2023.132729

Yakubu, M., Vwavware, J.O., Ojobeagu, A.O. & Ohwofosirai, A. (2026). Detection and Characterization of Exoplanets using transit photometry. Nigerian journal of Applied Physics (NJAP), vol.2 (2), pp 37-48.